Supporting Information (Online Material) for

Anisotropic Thermal Expansion and a Second-order Charge Order Transition in the Ferrimagnetic $Dy_2CuZnMn_4O_{12}$ Perovskite with Triple A-site Cation Ordering

Alexei A. Belik*

Research Center for Materials Nanoarchitectonics (MANA), National Institute for Materials Science (NIMS), Namiki 1-1, Tsukuba, Ibaraki 305-0044, Japan

E-mail: Alexei.Belik@nims.go.jp

Table S1. Selected Bond Lengths (*l* (Å) < 2.8 Å), Bond Angles (deg), Bond Valence Sums, BVS, and Distortion Parameters of MnO_6, Δ, in $Dy_2CuZnMn_4O_{12}$ at 100 K [a]

Dy1–O5 ×2	2.289(9)	Dy2–O2 ×2	2.336(9)
Dy1–O3 ×2	2.340(8)	Dy2–O4 ×2	2.378(9)
Dy1–O2 ×2	2.400(9)	Dy2–O5 ×2	2.418(9)
Dy1–O1 ×4	2.656(7)	Dy2–O1 ×4	2.641(7)
BVS($Dy1^{3+}$)	+3.39	BVS($Dy2^{3+}$)	+3.18
Cu–O1 ×4	1.951(3)	Zn–O3 ×2	1.965(9)
BVS(Cu^{2+})	+1.92	Zn–O4 ×2	2.044(9)
		BVS(Zn^{2+})	+1.79
Mn1–O2 ×2	1.890(2)	Mn2–O5 ×2	1.901(2)
Mn1–O3 ×2	1.963(3)	Mn2–O4 ×2	1.932(3)
Mn1–O1 ×2	2.129(7)	Mn2–O1 ×2	1.946(8)
BVS($Mn1^{3+}$)	+3.30	BVS($Mn2^{4+}$)	+3.76
Δ(Mn1–O)	25.0×10^{-4}	BVS($Mn2^{3+}$)	+3.84
		Δ(Mn2–O)	1.0×10^{-4}
Mn1–O1–Mn2 ×2	144.84(9)	Mn2–O4–Mn2	139.94(9)
Mn1–O2–Mn1	147.53(9)	Mn2–O5–Mn2	145.03(9)
Mn1–O3–Mn1	134.91(9)		

[a] BVS = $\sum_{i=1}^{N} v_i$, $v_i = \exp[(R_0 - l_i)/B]$, N is the coordination number, $B = 0.37$, $R_0(Dy^{3+}) = 2.036$, $R_0(Cu^{2+}) = 1.679$, $R_0(Zn^{2+}) = 1.704$, $R_0(Mn^{4+}) = 1.753$, and $R_0(Mn^{3+}) = 1.76$.

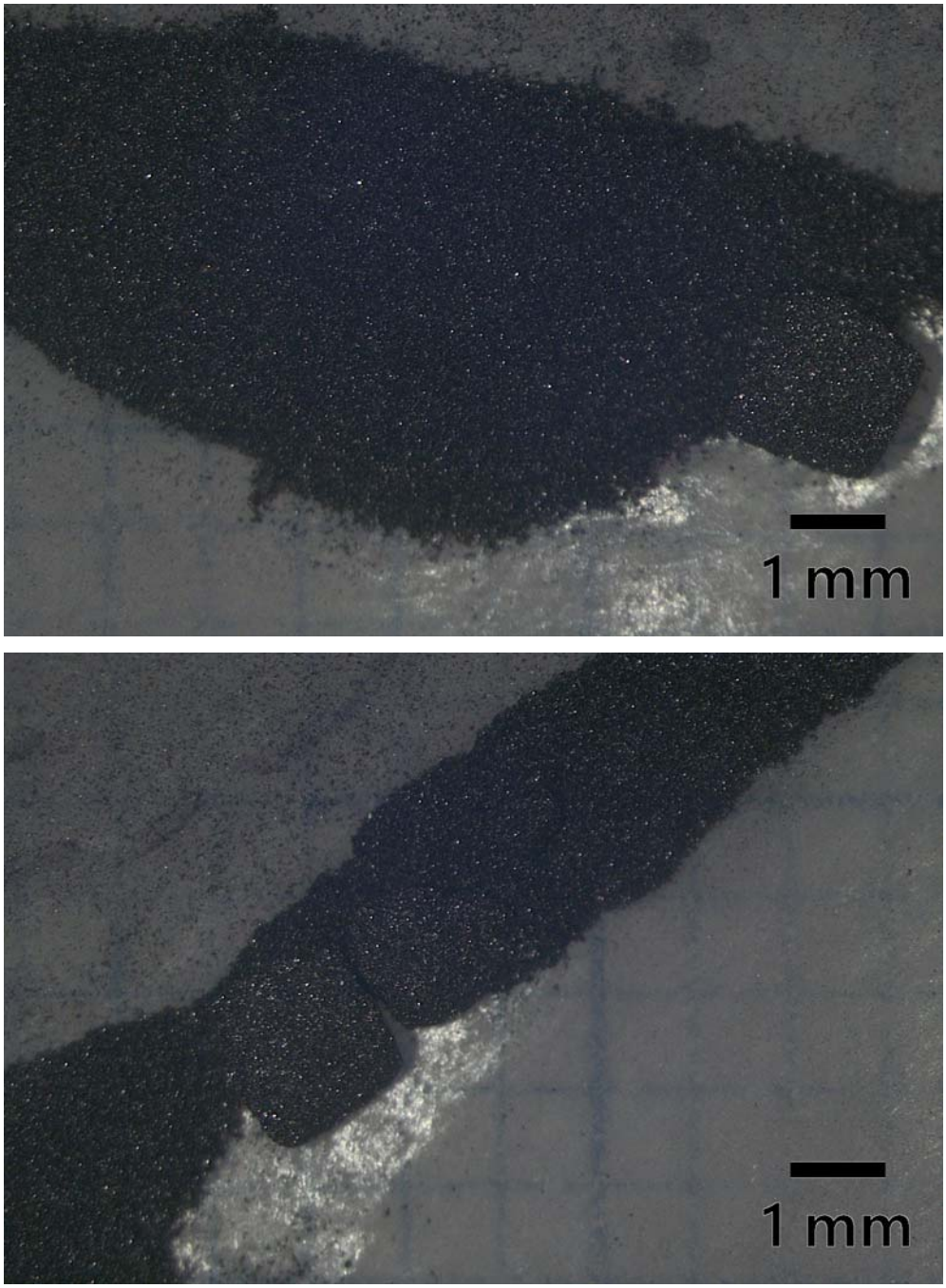

Figure S1. Photographs of the as-synthesized $Dy_2CuZnMn_4O_{12}$ sample. This figure shows that the as-synthesized sample was a highly fragile pellet, which fell into powder when touched.

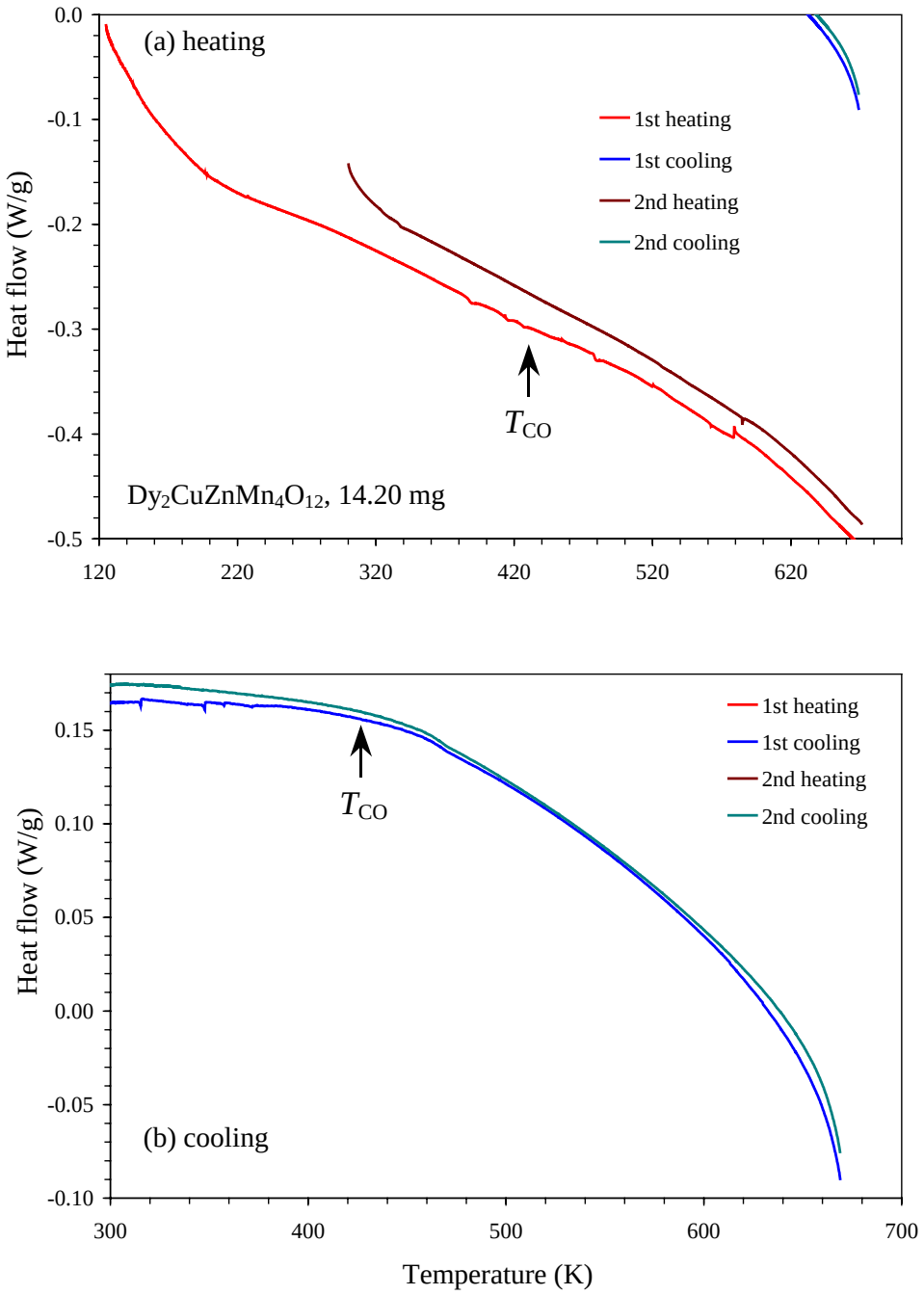

Figure S2. Differential scanning calorimetry (DSC) curves of a powder sample of $Dy_2CuZnMn_4O_{12}$ (14.20 mg) on (a) heating and (b) cooling. The arrows show the charge-order phase transition temperature determined by high-temperature synchrotron X-ray powder diffraction – no anomalies were detected at this temperature by DSC.

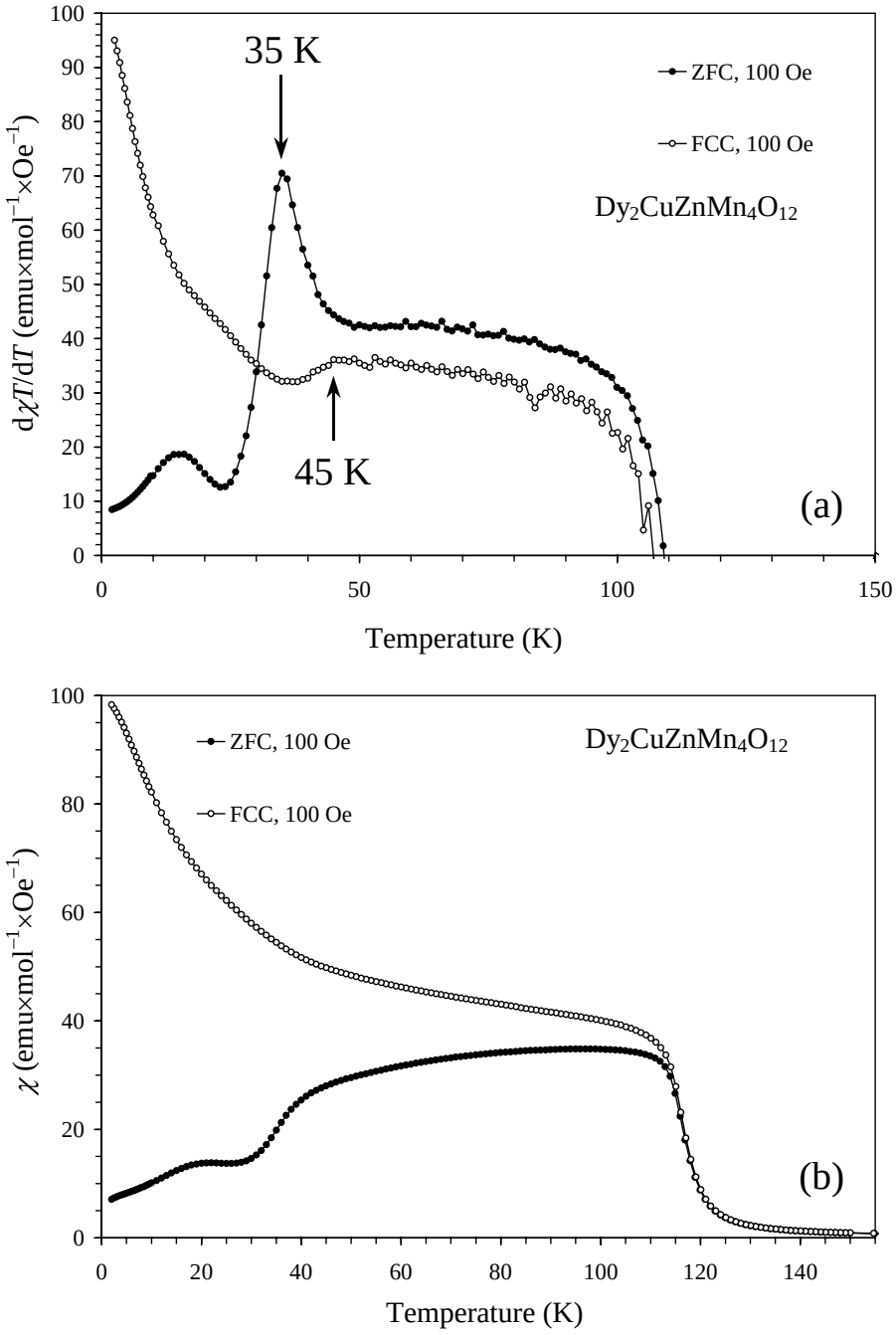

Figure S3. (a) A fragment of the ZFC and FCC dχT/dT versus T curves of $Dy_2CuZnMn_4O_{12}$ at H = 100 Oe to emphasize anomalies near 35–45 K. (b) The ZFC and FCC χ versus T curves of $Dy_2CuZnMn_4O_{12}$ at H = 100 Oe below 155 K.

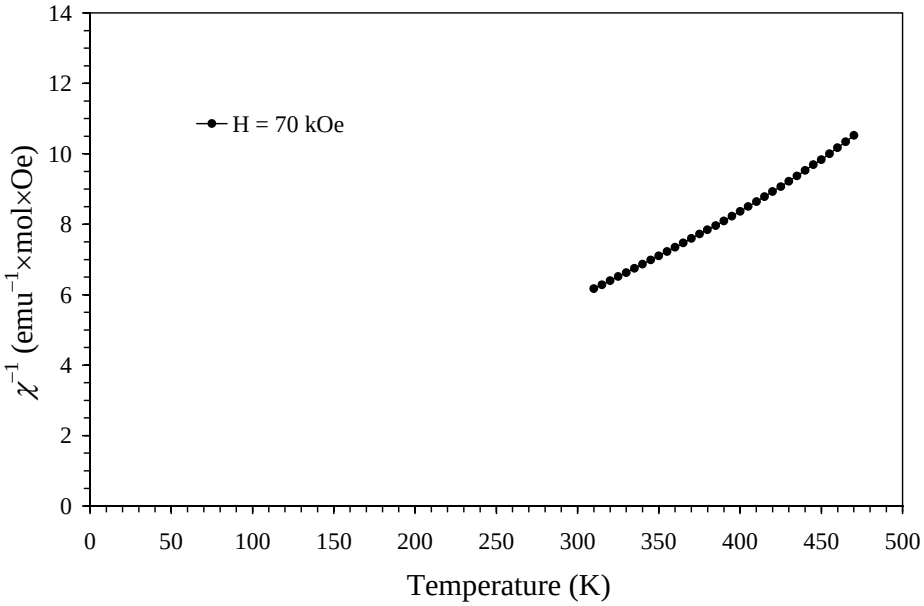

Figure S4. (Raw/uncorrected) high-temperature inverse χ^{-1} versus T curve of $Dy_2CuZnMn_4O_{12}$ at H = 70 kOe measured from 300 K to 470 K. A small deviation from the linear behavior at high temperatures is caused by a temperature-independent contribution from a sample holder. There were no detectable anomalies near T_{CO} = 425 K.

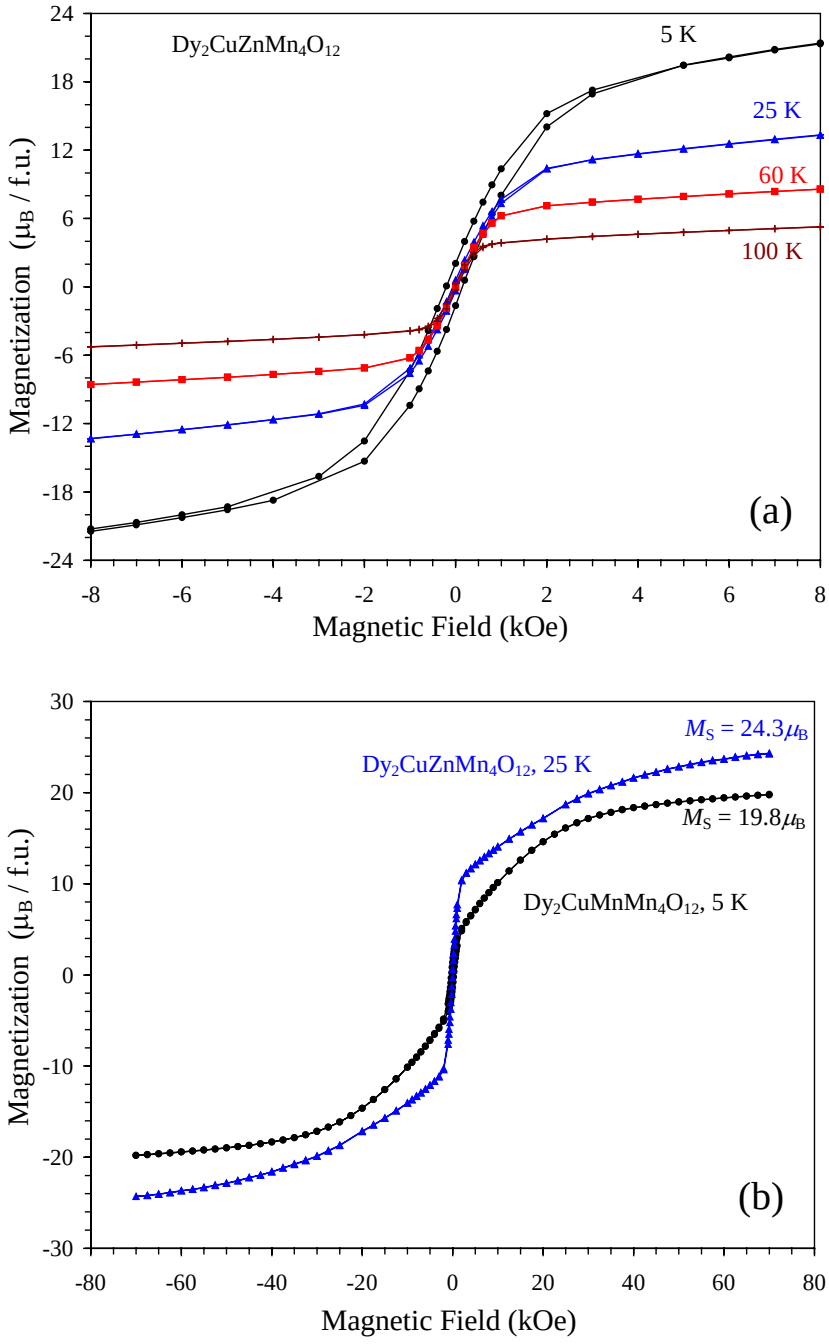

Figure S5. (a) A zoomed part of the *M* versus *H* curves of $Dy_2CuZnMn_4O_{12}$ at *T* = 5 K, 25 K, 60 K, and 100 K. (b) Comparison of the *M* versus *H* curves of $Dy_2CuZnMn_4O_{12}$ at *T* = 25 K (blue triangles) and $Dy_2CuMnMn_4O_{12}$ at *T* = 5 K (black circles) – the curves were qualitatively similar.

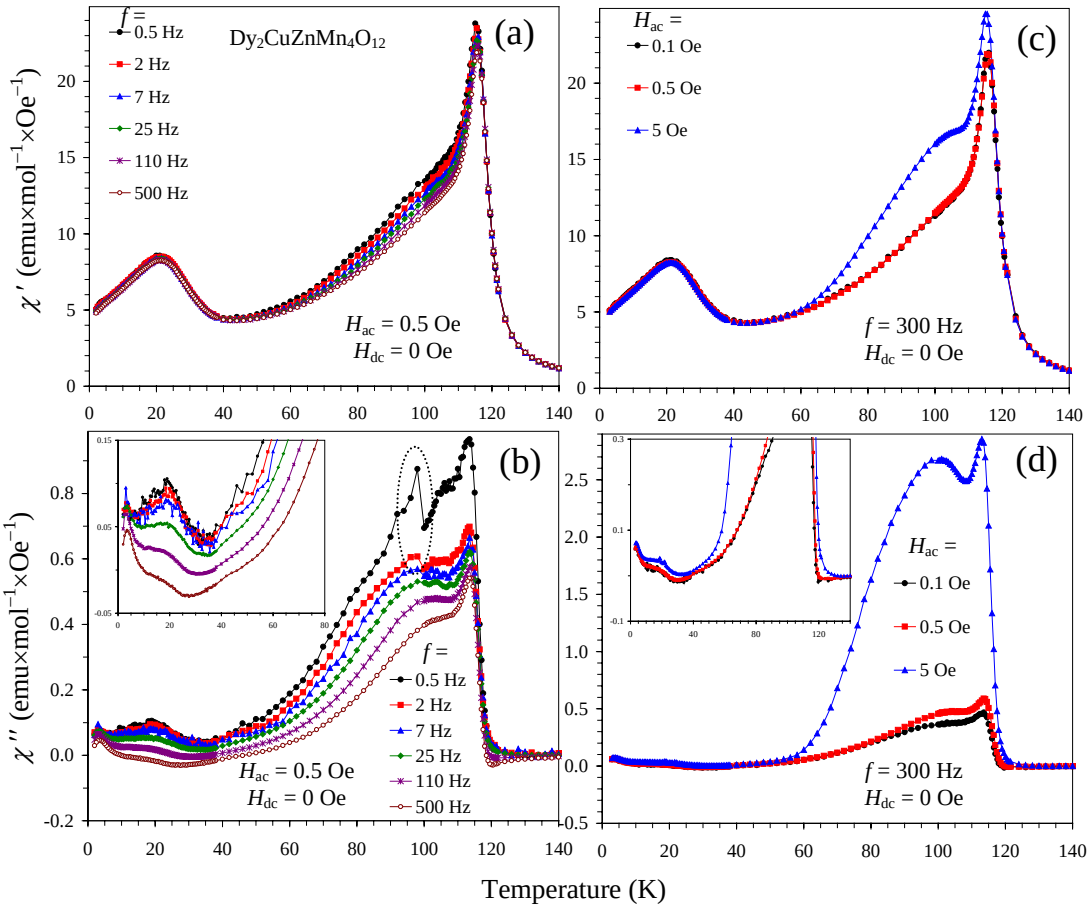

Figure S6. (a) The χ' versus T and (b) χ'' versus T curves of $Dy_2CuZnMn_4O_{12}$ at different frequencies measured with H_{ac} = 0.5 Oe and H_{dc} = 0 Oe. (c) The χ' versus T and (d) χ'' versus T curves at different H_{ac} = 0.1, 0.5, and 5 Oe and one frequency of 300 Hz (H_{dc} = 0 Oe). Insets show zoomed parts of the corresponding figures. The dotted oval on panel (b) emphasizes (most probably) measurement artifacts because the measurement steps changed exactly at this temperature range.